Transport in Porous Media (2025) 152:109
https://doi.org/10.1007/s11242-025-02249-2

# Laminar Forced Convection in a Porous Circular Microduct with Wall Roughness Effects

**M. Celli**[1] · **A. Barletta**[1]

Received: 31 May 2025 / Accepted: 21 October 2025 / Published online: 6 November 2025


**Abstract**
The study presented in this paper is devoted to the laminar forced convection heat transfer in a porous microduct with a circular cross section. At small cross-section scales, the effects of roughness at the duct walls may be important for the evaluation of the heat transfer rate. The analysis aims to provide the Nusselt number as a quantity dependent on the boundary shape uncertainty by averaging over statistical samples of microducts having different roughness distributions generated randomly. Each statistical sample refers to a prescribed ratio between the maximum size of the wall roughness and the microduct nominal radius, and to a prescribed number of nodes employed to draw the boundary shape. Boundary conditions of either uniform wall temperature (T condition) or wall heating (H1 or H2 conditions) are considered. The results show that both the roughness and the number of nodes defining the microduct cross-sectional shape tend to inhibit the heat transfer: a sufficiently high value of the roughness amplitude may halve the Nusselt number relative to the smooth case. The Nusselt number obtained for the H2 condition decreases faster with the roughness amplitude compared with the Nusselt number obtained for the T and H1 conditions.

**Keywords** Microduct · Porous medium · Darcy's flow · Forced convection · Wall roughness · Nusselt number

**List of Symbols**

| | |
|---|---|
| $a$ | Constant streamwise temperature gradient |
| $Br$ | Brinkman number |
| $c$ | Specific heat of the fluid |
| $\mathrm{d}s$ | Infinitesimal line element |
| $\hat{\mathbf{e}}_z$ | Unit vector in $z$ direction |

corresponding author.

✉ M. Celli
michele.celli3@unibo.it

A. Barletta
antonio.barletta@unibo.it

[1] Department of Industrial Engineering, University of Bologna, Viale Risorgimento 2, 40136 Bologna, Italy

| | |
|---|---|
| $K$ | Permeability |
| $n$ | Integer number |
| $\hat{\mathbf{n}}$ | Unit vector in outward normal direction |
| $N$ | Number of nodes |
| $Nu$ | Nusselt number |
| $\mathcal{P}$ | Rough boundary perimeter |
| $r_0$ | Microduct radius |
| $r$ | Radial coordinate |
| $\mathcal{S}$ | Rough cross-section surface |
| $T$ | Temperature |
| $\mathbf{u} = \{u, v, w\}$ | Velocity vector |
| $\mathbf{x} = \{x, y, z\}$ | Cartesian coordinates |
| $\{x_n, y_n\}$ | Position of $n^{th}$ node |

**Greek Symbols**

| | |
|---|---|
| $\alpha_m$ | Average thermal diffusivity |
| $\gamma$ | Dimensionless roughness amplitude |
| $\delta r_n$ | Dimensional roughness amplitude |
| $\theta_n$ | Angle of the $n^{th}$ node |
| $\kappa_m$ | Average thermal conductivity |
| $\mu$ | Dynamic viscosity of the fluid |
| $\xi$ | Dimensionless streamwise temperature gradient |
| $\rho$ | Density of the fluid |

**Superscript, subscripts**

| | |
|---|---|
| | Dimensionless quantity |
| $w$ | Wall |
| $b$ | Bulk |
| T, H1, H2 | − thermal boundary conditions |
| – | – |
| – | – |

## 1 Introduction

The study of convective heat transfer in porous media is a topic which deserves attention due to its wide-ranging applications in engineering systems such as geothermal reservoirs, thermal insulation, chemical reactors, and energy storage devices, as deeply reviewed by Nield and Bejan (2017). Among the possible configurations of interest, flow through fluid saturated porous media holds particular interest in scenarios where compact heat exchangers are involved.

Besides the porous media, also the use of microchannels has been widely considered to enhance the heat transfer performances of heat exchangers (Yarin et al. 2009; Cotta et al. 2016; Kandlikar et al. 2005). Since the compactness of innovative heat exchangers is a key feature, the literature recently displayed interest for the investigation of the heat transfer performances of fluid saturated porous microchannels (Farahani et al. 2021; Wang et al. 2022). The chance of treating the heat and mass transfer in porous microchannels by employing the usual local balances based on the reference elementary volume average procedure is ensured by the

chance of producing porous media with nanometric porous size, as reported in the review by Ying et al. (2022). The production of microchannels with very small hydraulic diameters, particularly below several tens of micrometers, can introduce uncertainties in their intended cross-section shape. At these scales, wall roughness becomes a significant factor affecting channel characteristics (Joy et al. 2023; Imaizumi et al. 2024; Akbari et al. 2023). Even minimal surface irregularities, in fact, can alter the velocity profile, promote recirculation zones, and enhance mixing, all of which directly influence the heat and mass transfer.

Recent papers have been published by Barletta et al. (2025) and by Sphaier et al. (2025) on the effect of roughness for the heat and mass transfer in microducts clear of porous media for fully developed flows, namely a two-dimensional analysis. They found that the roughness depresses the heat transfer performances and increases the pressure drop. The literature does not display a unique opinion on the influence of roughness on heat transfer. Three-dimensional simulations of rough ducts, in fact, found that the roughness, under certain conditions, may promote the increase of heat transfer performances because of the flow disruption that produces (Panda and Kumar 2021).

Forced convection heat transfer in ducts filled by a porous medium has been explored in several papers by Nield et al. (2002), by Nield et al. (2003), by Nield and Kuznetsov (2004), by Kuznetsov and Nield (2006a, 2006b) and by Kuznetsov and Nield (2010). The results of these analyses, mainly focused on the application of the classical theory of internal flow forced convection to the area of porous media, have been surveyed in Chapter 4 of the book by Nield and Bejan (2017).

The aim of this paper is the investigation of wall roughness effect on heat transfer in a two-dimensional fluid saturated porous microchannel with nominal circular cross section by analyzing the quantitative impacts of different roughness configurations. The flow is considered developed both hydrodynamically and thermally. Darcy's law is employed to model the momentum transport. This implies assuming relatively low velocities for the fluid and relatively low porosities for the solid matrix. For these reasons, the fluid saturated porous medium is assumed to be in local thermal equilibrium and a single-temperature energy balance equation is indeed employed to model the heat transfer. A finite-element method simulation is performed by using a commercial code for the solution of the local momentum and energy balance equation. A analysis of wide statistical samples of different circular cross sections affected by random roughness at the wall is performed. The results suggest that the roughness tends to depress the heat transfer performances.

## 2 Mathematical Model

Let us a consider a microduct with a circular cross section having radius $r_0$. The length of the microduct is considered as much larger than the radius, so that the flow can be considered as a fully developed Darcy's flow with a uniform seepage velocity $\mathbf{u} = u\,\hat{\mathbf{e}}_z$, where $u$ is the velocity component along the axis of the duct, denoted as $z$, and $\hat{\mathbf{e}}_z$ is the unit vector along the $z$ direction. The coordinates in the plane of the cross section are $(x, y)$.

The surface roughness of the microduct impermeable wall is modeled by assuming a deformation of the nominal circular boundary to a polygonal path, hereafter denoted as $\mathcal{P}$, having $N$ nodes, defined so that the positions $(x_n, y_n)$ of each node are given by

$$x_n = \left(r_0 + \delta r_n\right)\cos\theta_n, \qquad y_n = \left(r_0 + \delta r_n\right)\sin\theta_n, \qquad \text{for} \quad n = 1, \ldots N, \tag{1}$$

with the quantities $\delta r_n$ and $\theta_n$ are random values such that

$$-\gamma r_0 \le \delta r_n \le \gamma r_0, \qquad \frac{2(n-1)\pi}{N} < \theta_n < \frac{2n\pi}{N}, \tag{2}$$

where $\gamma > 0$ is the prescribed dimensionless roughness parameter which, at least theoretically, is constrained to be in the range $0 \le \gamma < 1$, even if we will not consider cases where $\gamma > 0.2$. The microduct cross section, bounded by $\mathcal{P}$, is denoted by $\mathcal{S}$. Two examples of the resulting cross section for fixed value of $\gamma = 0.1$ are reported in Figure 1: the left-hand side frame is obtained for $N = 50$ while the right-hand side frame is obtained for $N = 150$.

### 2.1 The Local Energy Balance

At the microscale, the effects of viscous dissipation may be important even at moderate flow rates. This means that the local energy balance equation, under steady-state regime, can be written as

$$u\,\frac{\partial T}{\partial z} = \alpha_m \nabla^2 T + \frac{\mu\, u^2}{K \rho\, c}, \tag{3}$$

where $T$ is the temperature field, $\alpha_m$ is the average thermal diffusivity of the fluid saturated porous medium, $K$ is its permeability, while $\rho$ and $c$ are the constant density and specific heat of the fluid. We will explore the fully developed temperature field, so that there exists a constant $a$ such that

$$\frac{\partial T}{\partial z} = a. \tag{4}$$

Hence, (3) can be rewritten as

$$\nabla^2 T = \frac{a\, u}{\alpha_m} - \frac{\mu\, u^2}{K \kappa_m}, \tag{5}$$

where $\kappa_m = \rho\, c\, \alpha_m$ is the average thermal conductivity of the fluid saturated porous medium.

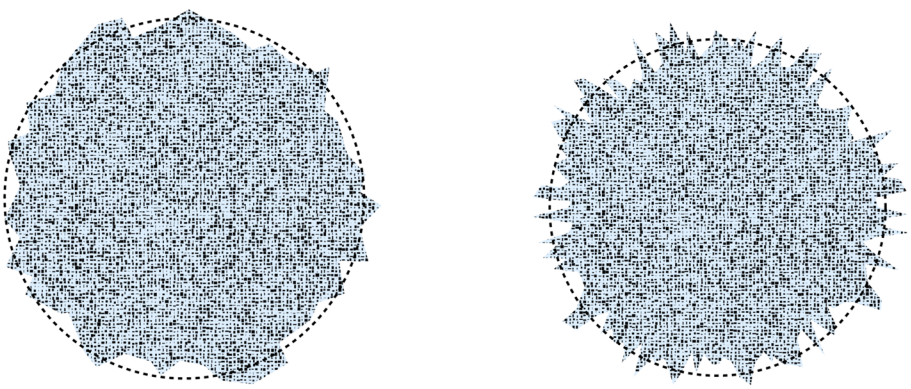

**Fig. 1** Examples of cross section for randomly generated roughness with $\gamma = 0.1$: the left-hand side frame refers to a shape produced by employing 50 nodes, $N = 50$; the right-hand side frame refers to a shape produced by employing 150 nodes, $N = 150$

### 2.2 The Thermal Boundary Conditions

The conditions to be prescribed for the temperature at the boundary $\mathcal{P}$ are of two types:

$$\begin{aligned}
&\mathsf{T} \text{ boundary conditions}: \quad (x,y)\in\mathcal{P} \implies T = T_w, \qquad a = 0,\\
&\mathsf{H1} \text{ boundary conditions}: \quad (x,y)\in\mathcal{P} \implies T = T_w, \qquad a \neq 0,\\
&\mathsf{H2} \text{ boundary conditions}: \quad (x,y)\in\mathcal{P} \implies \kappa_m\,\hat{\mathbf{n}}\cdot\boldsymbol{\nabla}T = q_w, \qquad a \neq 0,
\end{aligned} \tag{6}$$

where the wall temperature $T_w$ depends only on $z$, for the $\mathsf{T}$ and $\mathsf{H1}$ conditions, so that

$$\frac{\partial T}{\partial z} = \frac{\mathrm{d}T_w}{\mathrm{d}z} = a, \tag{7}$$

as a consequence of (4) and (6). Furthermore, for the $\mathsf{H2}$ condition, the wall heat flux $q_w$ is a constant. We mention that the terminology of $\mathsf{T}$, $\mathsf{H1}$ and $\mathsf{H2}$ boundary conditions comes from the classical book by Shah and London (1978). On referring the reader to that book for further details, we just mention that the $\mathsf{T}$ condition models a case where the boundary temperature is uniform both perimetrally along $\mathcal{P}$ and in the $z$ direction, while the $\mathsf{H1}$ condition serves to describe wall heating with a highly conducting wall. In the $\mathsf{H1}$ case, the temperature is uniform perimetrally but it changes linearly with $z$. The $\mathsf{H2}$ condition describes constant wall heating with a value of $q_w$ which is uniform both perimetrally and in the $z$ direction. The difference between the $\mathsf{H1}$ and the $\mathsf{H2}$ conditions is that, in the former case, $q_w$ is not perimetrally uniform.

### 2.3 Nondimensional Formulation

We define the dimensionless quantities, denoted with asterisks,

$$\begin{aligned}
&(x^*,y^*) = \frac{(x,y)}{r_0}, \qquad \boldsymbol{\nabla}^* = r_0\boldsymbol{\nabla}, \qquad \nabla^{*2} = r_0^2\nabla^2, \qquad T^* = \kappa_m\frac{T-T_w}{q_w r_0},\\
&Br = \frac{\mu\,u^2 r_0}{2Kq_w}, \qquad \xi = \frac{\rho\,c\,r_0\,a\,u}{q_w},
\end{aligned} \tag{8}$$

where $r_0$ is microduct radius, $Br$ is Darcy's law version of the Brinkman number and $\xi$ is the dimensionless streamwise temperature gradient. We note that the Brinkman number defines non-dimensionally the strength of the internal heating due to viscous dissipation. Furthermore, in general, symbol $q_w$ denotes the perimetrally averaged heat flux supplied to the flowing fluid,

$$q_w = \frac{\kappa_m}{\mathcal{P}}\int_{\mathcal{P}}\hat{\mathbf{n}}\cdot\boldsymbol{\nabla}T\,\mathrm{d}s, \tag{9}$$

where, hereafter, $\mathcal{P}$ denotes both the perimeter of the microduct cross section and its length, $\hat{\mathbf{n}}$ is the outward unit normal to $\mathcal{P}$ and $\mathrm{d}s$ is the infinitesimal line element along $\mathcal{P}$. Likewise, $\mathcal{S}$ denotes both the region in the $(x, y)$ plane and the area of the microduct cross section.

Equations (7) and (9) allow one to draw the fundamental property of fully developed forced convection in internal flows: both $T - T_w$ and $q_w$ do not depend on $z$. As a consequence, the dimensionless temperature field $T^*$, defined by (8), depends just on $x^*$ and $y^*$ or, in other words, is two-dimensional.

Equation (5) can be rewritten in a nondimensional formulation as

$$\nabla^{*2} T^* = \xi - 2Br, \tag{10}$$

where $\nabla^{*2}$ is intended as a two-dimensional Laplacian in the $(x^*, y^*)$ plane. By employing (8), (9) and the Gauss-Green theorem, an integration of (10) over $\mathcal{S}^*$ yields

$$\xi - 2Br = \frac{\mathcal{P}^*}{\mathcal{S}^*}, \tag{11}$$

where $\mathcal{S}^*$ and $\mathcal{P}^*$ are the nondimensional counterparts of $\mathcal{S}$ and $\mathcal{P}$, respectively, obtained by rescaling the coordinates $(x, y)$ by $r_0$.

The boundary conditions (6) can be rewritten as

$$\begin{aligned}
&\mathsf{T} \text{ boundary conditions}: \quad (x^*, y^*) \in \mathcal{P}^* \implies T^* = 0, \qquad \xi = 0, \\
&\mathsf{H1} \text{ boundary conditions}: \quad (x^*, y^*) \in \mathcal{P}^* \implies T^* = 0, \qquad \xi \neq 0, \\
&\mathsf{H2} \text{ boundary conditions}: \quad (x^*, y^*) \in \mathcal{P}^* \implies \hat{\mathbf{n}} \cdot \boldsymbol{\nabla}^* T^* = 1, \qquad \xi \neq 0.
\end{aligned} \tag{12}$$

In the case of the boundary condition $\mathsf{T}$, one has a constrained value of the Brinkman number $Br = Br_0$ obtained from (11) by setting $\xi = 0$,

$$Br_0 = -\frac{\mathcal{P}^*}{2\mathcal{S}^*}, \tag{13}$$

while, in the case of the boundary condition $\mathsf{H1}$, the value of $\xi$ is determined from (11) for every prescribed value of $Br$. Another fundamental dimensionless parameter for the forced convection heat transfer analyses is the Nusselt number, given by

$$Nu = \frac{2 r_0 \, q_w}{\kappa_m \left( T_w - T_b \right)}, \tag{14}$$

where $T_b$ is the bulk temperature. In the case of Darcy's flow, as the velocity profile is uniform, the bulk temperature is just the mean temperature over the microduct cross section,

$$T_b = \frac{1}{\mathcal{S}} \iint_{\mathcal{S}} T \, \mathrm{d}x \, \mathrm{d}y. \tag{15}$$

On account of (14) and (15), one may write

$$Nu = -\frac{2}{T_b^*}, \qquad \text{for} \quad T_b^* = \frac{1}{\mathcal{S}^*} \iint_{\mathcal{S}^*} T^* \, \mathrm{d}x^* \, \mathrm{d}y^*. \tag{16}$$

By employing (10)-(12) and (16), one may draw three important conclusions:

- The dimensionless temperature $T^*$ and the Nusselt number $Nu$ depend just on the domain $\mathcal{S}^*$ and on its boundary $\mathcal{P}^*$, but they do not depend individually on either $\xi$ or $Br$.
- The dimensionless temperature $T^*$ and the Nusselt number $Nu$ are the same for the boundary conditions $\mathsf{T}$ and $\mathsf{H1}$, the only difference is that $Br = Br_0$ in the former case while, in the latter case, it can be prescribed arbitrarily.
- In general, $T^*$ and $Nu$ for the $\mathsf{H2}$ condition differs from those relative to the $\mathsf{T}$ and $\mathsf{H1}$ conditions.

Such conclusions mark a net discrepancy with the case of clear fluid flow (Barletta et al. 2025). For that case, the fully developed values of *Nu* turned out to depend on *Br* both for the H1 and the H2 boundary conditions.

### 2.4 The Smooth Circular Duct

When the wall roughness is absent, so that $\mathcal{P}$ is a circumference with radius $r_0$, then the solution of the forced convection problem is trivial. Indeed, the rotational symmetry of the cross-section region implies that the H1 and H2 boundary conditions coincide in this special case. Equations (10) and (12) yield

$$T^* = \frac{1}{2}\left(r^{*2} - 1\right), \qquad \text{for} \quad r^* = \left(x^{*2} + y^{*2}\right)^{1/2}. \tag{17}$$

In fact, when the cross section is perfectly circular, we have $\mathcal{S}^* = \pi$ and $\mathcal{P}^* = 2\pi$ so that (11) yields $\xi - 2Br = 2$. From, (16) and (17), one eventually obtains

$$T_b^* = -\frac{1}{4}, \qquad Nu = 8. \tag{18}$$

The results displayed in (17) and (18) hold for the T condition, for the H1 condition and for the H2 condition. As already pointed out, such results are not influenced by the value of *Br*, even if for the T condition we have a constrained value, $Br = Br_0$, where $Br_0 = -1$ as implied by (13).

## 3 Analysis of the Wall Roughness Effects

### 3.1 Code Validation

The effect of the wall roughness is investigated numerically by solving the dimensionless local energy balance equation obtained by combining Equations (10) and (11), namely

$$\nabla^{*2} T^* = \frac{\mathcal{P}^*}{\mathcal{S}^*}. \tag{19}$$

The solution of Equation (19) is obtained by employing the finite-element method solver which is part of the software system *Wolfram 14.1* (©Wolfram Research Inc.). The solver is one of the possible solvers embedded in the function called *NDSolve*. The mesh employed to discretise the domain is unstructured and with triangular elements. The number of triangular elements employed changes for every cross section generated: the mesh independence test has been performed by checking the results versus the mesher option *MaxCellMeasure*. This option specifies the maximum value of the area of a single triangular element. Table 1 displays the behavior of *Nu* for decreasing values of *MaxCellMeasure* and for fixed cross section. The cross-section type chosen for the mesh independence test is the one reported on the right-hand side of Figure 1, namely a cross section characterized by $\gamma = 0.1$ and $N = 150$. In the following analysis, for every set values of dimensionless roughness $\gamma$ and number of nodes $N$, a statistical sample of 500 different cross sections is employed. Given the computational needs, the best agreement between accuracy and computational effort yields a choice of $10^{-3}$ for the value of *MaxCellMeasure*.

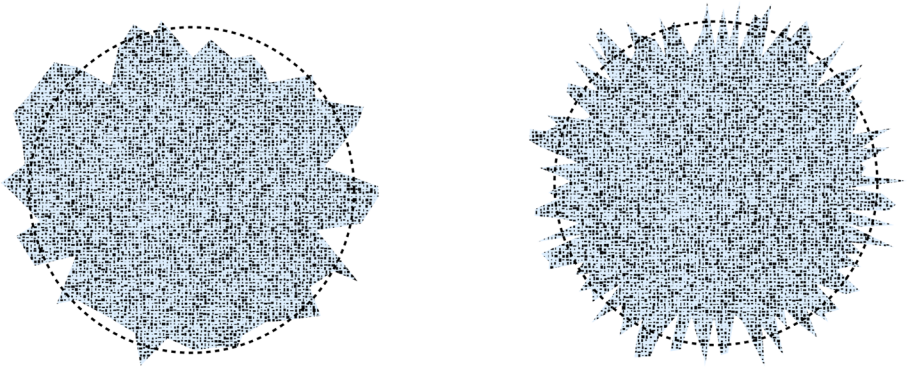

**Fig. 2** Examples of cross section with $\gamma = 0.2$: the left-hand side frame is drawn for $N = 50$; the right-hand side frame is drawn for $N = 150$

**Table 1** Values of Nusselt number obtained for a given cross section, drawn for $\gamma = 0.1$ and $N = 150$, as function of the *MaxCellMeasure* value for both the cases T/H1 and H2

| Max Cell Measure | $Nu_{\mathrm{T,H1}}$ | $Nu_{\mathrm{H2}}$ |
|---|---|---|
| $1 \cdot 10^{-2}$ | 4.7616 | 3.7151 |
| $5 \cdot 10^{-3}$ | 4.7585 | 3.7138 |
| $1 \cdot 10^{-3}$ | 4.7205 | 3.7054 |
| $5 \cdot 10^{-4}$ | 4.7112 | 3.7039 |
| $1 \cdot 10^{-4}$ | 4.7013 | 3.7020 |
| $5 \cdot 10^{-4}$ | 4.6989 | 3.7018 |

The limiting case of a smooth circular porous duct can be reproduced numerically by imposing $\gamma \to 0$. This behavior is evident in Tables 2 and 3. The literature value of the Nusselt number reported in (18) is indeed matched by the simulations with a good agreement. An exception is present for the case $N = 50$, where the number of nodes employed to draw the polygon is not sufficiently high to obtain a good approximation of the perfectly smooth circle.

### 3.2 Discussion of the Results

Each result reported in the following is obtained by setting $\gamma$ and $N$. For each prescription of $\gamma$ and $N$, a statistical sample composed by 500 simulations performed by using 500 different rough cross sections is considered. For every statistical sample, the average value of $Nu$ together with its relative standard deviation $\sigma$ is computed. For each $\gamma$ and $N$, two different values of Nusselt number and of the relative standard deviation are obtained: one for the thermal boundary conditions T/H1 and the other for the thermal boundary condition H2.

Values of dimensionless roughness amplitude $\gamma > 0.1$ imply a severe modification of the nominal circular cross-section shape of the channel. In Figure 2, the case $\gamma = 0.2$ is displayed to better understand the geometry deformation for high values of $\gamma$. The choice of considering such high values of $\gamma$ aims to obtain both a better comprehension of the

**Table 2** Average values of Nusselt number and the relative standard deviation for the cases T/H1 versus the dimensionless roughness $\gamma$ for three different values of the number of nodes $N$

| | $Nu_{T,H1}$ | | | $\sigma_{T,H1}$ | | |
|---|---|---|---|---|---|---|
| $\gamma$ | $N = 50$ | $N = 100$ | $N = 150$ | $N = 50$ | $N = 100$ | $N = 150$ |
| 0 | 8.01 | 8.00 | 8.00 | 0.000717 | 0.000109 | 0.0000374 |
| 0.005 | 8.01 | 7.98 | 7.96 | 0.00374 | 0.00420 | 0.00631 |
| 0.01 | 7.99 | 7.93 | 7.84 | 0.00800 | 0.0118 | 0.0204 |
| 0.05 | 7.73 | 6.98 | 6.18 | 0.0661 | 0.119 | 0.137 |
| 0.07 | 7.52 | 6.48 | 5.49 | 0.0996 | 0.143 | 0.150 |
| 0.1 | 7.25 | 5.84 | 4.74 | 0.152 | 0.176 | 0.164 |
| 0.12 | 7.07 | 5.51 | 4.40 | 0.174 | 0.213 | 0.169 |
| 0.15 | 6.85 | 5.13 | 4.04 | 0.197 | 0.195 | 0.165 |
| 0.16 | 6.80 | 5.07 | 3.95 | 0.211 | 0.208 | 0.162 |
| 0.17 | 6.73 | 4.98 | 3.89 | 0.219 | 0.214 | 0.167 |
| 0.18 | 6.67 | 4.92 | 3.82 | 0.220 | 0.215 | 0.163 |
| 0.19 | 6.64 | 4.85 | 3.77 | 0.244 | 0.218 | 0.169 |
| 0.2 | 6.62 | 4.81 | 3.73 | 0.227 | 0.216 | 0.165 |

**Table 3** Average values of Nusselt number and the relative standard deviation for the case H2 versus the dimensionless roughness $\gamma$ for three different values of the number of nodes $N$

| | $Nu_{H2}$ | | | $\sigma_{H2}$ | | |
|---|---|---|---|---|---|---|
| $\gamma$ | $N = 50$ | $N = 100$ | $N = 150$ | $N = 50$ | $N = 100$ | $N = 150$ |
| 0 | 8.01 | 8.00 | 8.00 | 0.000514 | 0.0000924 | 0.0000339 |
| 0.005 | 8.00 | 7.98 | 7.95 | 0.00376 | 0.00451 | 0.00686 |
| 0.01 | 7.99 | 7.92 | 7.82 | 0.00862 | 0.0133 | 0.0228 |
| 0.05 | 7.54 | 6.61 | 5.70 | 0.0910 | 0.153 | 0.162 |
| 0.07 | 7.16 | 5.85 | 4.76 | 0.147 | 0.189 | 0.176 |
| 0.1 | 6.57 | 4.83 | 3.71 | 0.242 | 0.235 | 0.189 |
| 0.12 | 6.17 | 4.28 | 3.21 | 0.280 | 0.259 | 0.194 |
| 0.15 | 5.56 | 3.61 | 2.64 | 0.337 | 0.251 | 0.180 |
| 0.16 | 5.40 | 3.46 | 2.49 | 0.353 | 0.261 | 0.172 |
| 0.17 | 5.19 | 3.27 | 2.35 | 0.363 | 0.263 | 0.170 |
| 0.18 | 5.01 | 3.13 | 2.23 | 0.380 | 0.267 | 0.160 |
| 0.19 | 4.86 | 2.97 | 2.12 | 0.404 | 0.254 | 0.160 |
| 0.2 | 4.75 | 2.85 | 2.01 | 0.387 | 0.255 | 0.158 |

influence of the roughness amplitude on $Nu$ and a more exhaustive analysis. We note that, from now on, for all figures presented the green refers to the case $N = 50$ while the red refers to the case $N = 100$ and the orange refers to the case $N = 150$.

One may point out, from Table 2, Table 3 and Figure 3, that the Nusselt number is, for every possible thermal boundary condition and for every prescribed value of $N$, a decreasing function of the roughness $\gamma$. This result is consistent with the results obtained for microducts clear of porous media and for the same boundary conditions by Barletta et al.

(2025) and by Sphaier et al. (2025). It is also evident, from the results reported, that $Nu$ is a decreasing function of $N$. The number of nodes $N$ has, in fact, a depressing influence on the values of the Nusselt number for every case considered as it can be clearly spotted by looking at Table 2, Table 3 and Figure 3.

In Figure 4, $\mathcal{P}^*/\mathcal{S}^*$ is presented as an increasing function of both $\gamma$ and $N$. This is a straightforward conclusion which could have been easily expected by looking at Figures 1 and 3: the perimeter $\mathcal{P}^*$ is, in fact, an increasing function of both the roughness and of the number of nodes employed to draw the cross section, while the area $\mathcal{S}^*$ slightly fluctuates around its nominal value.

One may also note that the Nusselt number for the case T/H1 is always equal or greater than that for the case H2. This result is consistent with the literature results by Shah and London (1978), by Barletta et al. (2025) and by Sphaier et al. (2025).

The interpretation of the influence of $\gamma$ on the variability of the Nusselt number over the statistical sample is also needed. The standard deviation, which captures the statistical dispersion in the values of $Nu$, is indeed an increasing function of $\gamma$ for sufficiently small values of $\gamma$ then it reaches a statistically stable value (except for the $N = 50$ cases), as reported in Figure 5. The standard deviation becomes independent of $\gamma$ at different values of $\gamma$ depending on the values of $N$ and on the case considered (T/H1 or H2). The reason why the standard deviation of the Nusselt number achieves a stabilization to certain values may be found in Figure 2. We recall that the left-hand side frame of Figure 2 is obtained by setting $N = 50$, while the right-hand side frame of Figure 2 is obtained by setting $N = 150$. One may note that, in the right-hand side frame of Figure 2, the cross-section boundary displays a random distribution of spikes drawn around the nominal radius. This suggests that no significant variability in the cross section can be obtained by producing cross sections with a sufficiently high $N$. On the other hand, when $N$ is sufficiently low, a case displayed in the left-hand side frame of Figure 2, one can infer that a random change in the

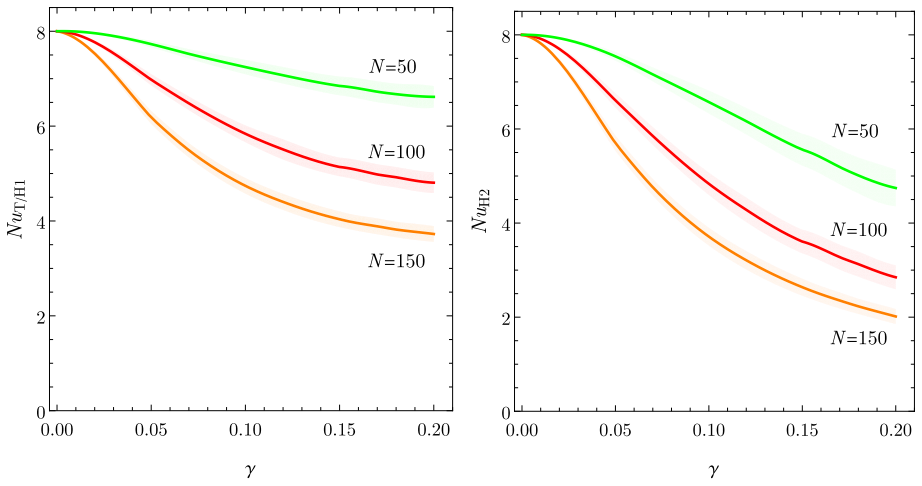


**Fig. 3** Nusselt number as function of the dimensionless roughness $\gamma$ for set values of $N$: the left-hand side frame refers to $Nu$ obtained for the case T/H1 while the right-hand side frame refers to $Nu$ obtained for the case H2. The green color refers to $N = 50$, the red refers to $N = 100$ and the orange refers to $N = 150$. The colored transparent bands display the standard deviation $\sigma$ of $Nu$

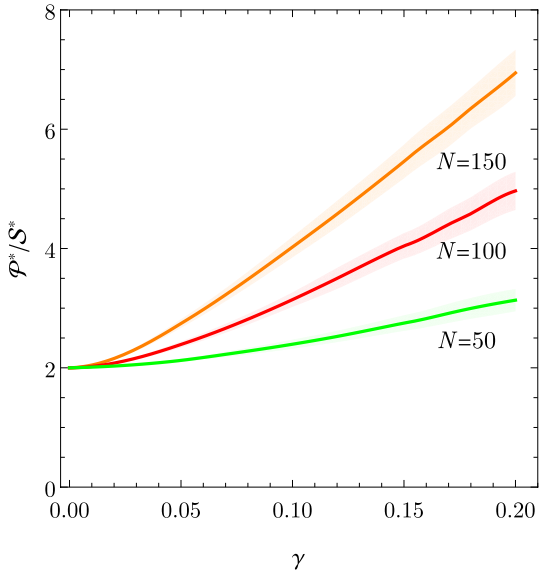


**Fig. 4** Values of $\mathcal{P}^*/\mathcal{S}^*$ as function of the dimensionless roughness $\gamma$ and for set values of $N$. The green color refers to $N = 50$, the red refers to $N = 100$ and the orange refers to $N = 150$. The colored transparent bands display the standard deviation $\sigma$ of $\mathcal{P}^*/\mathcal{S}^*$

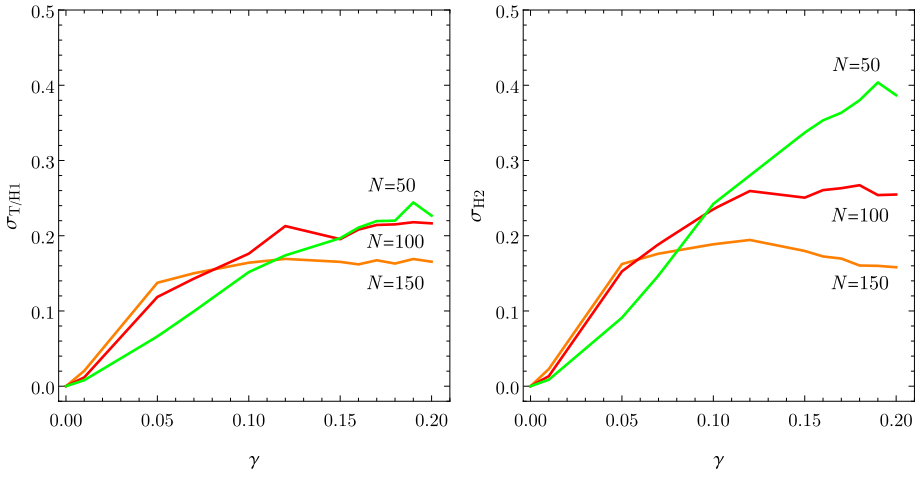


**Fig. 5** Standard deviation $\sigma$ of the Nusselt number as function of the dimensionless roughness $\gamma$ and for set values of $N$: the left-hand side frame refers to the case T/H1 while the right-hand side frame refers the case H2. The green color refers to $N = 50$, the red refers to $N = 100$ and the orange refers to $N = 150$

cross section would produce a significantly different shape which would also yield a variability in the computed Nusselt numbers.

Another interesting feature of the standard deviation of the Nusselt number behavior is being a decreasing function of $N$. This feature is particularly marked for the H2 thermal boundary condition case. This behavior may be interpreted by recalling that having a high number of nodes $N$ may yield, for sufficiently high values of $\gamma$, cross-section shapes characterized by the presence of large numbers of spikes. These configurations

approach a fractal-like morphology with a minor distinction between two different cross sections.

## 4 Conclusions

The statistical analysis of the influence of the cross-section rough shape of a fluid saturated microduct on the heat transfer performances is presented. The forced convection problem is studied assuming that the flow is fully developed both hydrodynamically and thermally. The small hydraulic diameter of the duct together with the presence of a porous medium justifies the choice of considering the effect of the heat generated by viscous dissipation as non-negligible.

There are different relevant conclusions which can be drawn:

- For given thermal boundary conditions, the dimensionless temperature field and the Nusselt number depend only on the cross-section geometry;
- The dimensionless temperature field and the Nusselt number are the same for the boundary conditions T and H1;
- The Nusselt number for the T/H1 case is always greater or equal than that for the H2 case;
- The Nusselt number is, both for T/H1 and H2 boundary conditions, a decreasing function of the roughness parameter: the heat transfer performance of the microduct is affected negatively by the presence of roughness at the boundary wall;
- The Nusselt number is a decreasing function of the number of nodes defining the cross-section shape of the microduct;
- The variability of the Nusselt number over the statistical sample, i.e., the standard deviation, is an increasing function of the roughness. When the surface roughness affects significantly the cross-section shape, then one experiences a significant difficulty in the prediction of the heat transfer performance of the microduct;
- The standard deviation tends to reach a stable value for a combination of sufficiently high roughness and of sufficiently large number of nodes. A large number of nodes yields, for increasing roughness, boundary walls characterized by a visually fractal-like shape. Once this condition is achieved, the standard deviation of the Nusselt number becomes stable. Conversely, a relatively small number of nodes yields an important variability in the cross-section shapes (especially for high values of roughness).

**Author Contributions** All authors contributed to the study conception, design, computation of the results, and to the writing. All authors read and approved the final manuscript.

**Funding** Open access funding provided by Alma Mater Studiorum - Università di Bologna within the CRUI-CARE Agreement. This work has been supported by Alma Mater Studiorum Universit di Bologna through the RFO 2024 research grant.

## Declarations

**Conflict of interest** The authors have no relevant financial or non-financial interests to disclose.

## References

Akbari, Z., Raoufi, M.A., Mirjalali, S., Aghajanloo, B.: A review on inertial microfluidic fabrication methods. Biomicrofluidics, **17**(5) (2023)

Barletta, A., Celli, M., Sphaier, L.A., Brandão, P.V., Lazzari, S., Ghedini, E.: Shape uncertainty analysis of laminar forced convection in a round microchannel with viscous dissipation. Appl. Therm. Eng. **265**, 125536 (2025)

Cotta, R.M., Knupp, D.C., Naveira-Cotta, C.P.: Analytical Heat and Fluid Flow in Microchannels and Microsystems. Springer (2016)

Farahani, S.D., Farahani, A.D., Hajian, E.: Effect of pcm and porous media/nanofluid on the thermal efficiency of microchannel heat sinks. Int. Commun. Heat Mass Transf. **127**, 105546 (2021)

Imaizumi, K., Fujita, A., Suzuki, A., Kobashi, M., Kato, M.: Additive manufacturing for 3D microchannel structure using $La(Fe_xSi_{1-x})_{13}$ magnetic refrigerant via laser powder bed fusion. Addit. Manuf. **83**, 104076 (2024)

Joy, A., Shiblemon, K., Baby, B.: Review on fabrication and experimental study of microchannel heat sinks for cooling of electronic components. Mater. Today: Proceed. **72**, 2985–2991 (2023)

Kandlikar, S., Garimella, S., Li, D., Colin, S., King, M.R.: Heat Transfer and Fluid Flow in Minichannels and Microchannels. Elsevier (2005)

Kuznetsov, A.V., Nield, D.A.: Forced convection with laminar pulsating flow in a saturated porous channel or tube. Transp. Porous Media **65**, 505–523 (2006a)

Kuznetsov, A.V., Nield, D.A.: Thermally developing forced convection in a bidisperse porous medium. Journal of Porous Media, **9** (2006b)

Kuznetsov, A.V., Nield, D.A.: Forced convection in a channel partly occupied by a bidisperse porous medium: asymmetric case. Int. J. Heat Mass Transf. **53**, 5167–5175 (2010)

Nield, D., Bejan, A.: Convection in Porous Media, 5th edn. Springer, New York (2017)

Nield, D.A., Kuznetsov, A.V.: Forced convection in a bi-disperse porous medium channel: a conjugate problem. Int. J. Heat Mass Transf. **47**, 5375–5380 (2004)

Nield, D.A., Kuznetsov, A.V., Xiong, M.: Effect of local thermal non-equilibrium on thermally developing forced convection in a porous medium. Int. J. Heat Mass Transf. **45**, 4949–4955 (2002)

Nield, D.A., Kuznetsov, A.V., Xiong, M.: Thermally developing forced convection in a porous medium: parallel plate channel with walls at uniform temperature, with axial conduction and viscous dissipation effects. Int. J. Heat Mass Transf. **46**, 643–651 (2003)

Panda, S., Kumar, R.: A review on effect of various artificial roughness on heat transfer enhancement in a channel flow. J. Therm. Eng. **7**, 1267–1301 (2021)

Shah, R.K., London, A.L.: Laminar Flow Forced Convection in Ducts. In Advances in Heat Transfer. Academic Press (1978)

Sphaier, L.A., Barletta, A., Celli, M., Brandão, P.V., Ghedini, E.: Laminar forced convection in circular microchannels with slip-flow: analysis of randomly distributed roughness. Int. Commun. Heat Mass Transf. **162**, 108615 (2025)

Wang, J., Xu, Y.-P., Qahiti, R., Jafaryar, M., Alazwari, M.A., Abu-Hamdeh, N.H., Issakhov, A., Selim, M.M.: Simulation of hybrid nanofluid flow within a microchannel heat sink considering porous media analyzing cpu stability. J. Petrol. Sci. Eng. **208**, 109734 (2022)

Yarin, L., Mosyak, A., Hetsroni, G.: Fluid flow, heat transfer and boiling in micro-channels. Springer (2009)

Ying, J., Lenaerts, S., Symes, M.D., Yang, X.-Y.: Hierarchical design in nanoporous metals. Advanced Science (Weinheim, Baden-wurttemberg, Germany), **9**, 2106117 (2022)